ACS APPLIED MATERIALS & INTERFACES

Research Article

www.acsami.org

Controlled Ti Seed Layer Assisted Growth and Field Emission Properties of $Pb(Zr_{0.52}Ti_{0.48})O_3$ Nanowire Arrays

Anuja Datta,*[,†] Devajyoti Mukherjee,[†,‡] Mahesh Hordagoda,[‡] Sarath Witanachchi,[†,‡] and Pritish Mukherjee[†,‡]

[†]Florida Cluster for Advanced Smart Sensor Technologies and Department of Physics, [‡]Center for Integrated Functional Materials and Department of Physics, University of South Florida, Tampa, Florida 33620, United States

Ranjit V. Kashid,[§] Mahendra A. More,[§] Dilip S. Joag,[§] and Padmakar G. Chavan[⊥]

[§]Centre for Advanced Studies in Materials Science and Condensed Matter Physics, Department of Physics, University of Pune, Pune 411007, India

[⊥]Department of Physics, School of Physical Sciences, North Maharashtra University, Jalgaon 425 001, India

ABSTRACT: We report on the directed upright growth of ferroelectric (FE) $Pb(Zr_{0.52}Ti_{0.48})O_3$ (PZT) nanowire (NW) arrays with large aspect ratios of >60 using a Ti seed layer assisted hydrothermal process over large surface areas on ITO/glass substrates. In a two-step growth process, Ti seed layer of low surface roughness with a thickness of ∼500 nm and grain size of ∼100 nm was first deposited by radio frequency (RF) sputtering which was subsequently used as substrates for the growth of highly dense, single crystalline PZT NWs by controlled nucleation. The electron emission properties of the PZT NWs were investigated using the as-grown NWs as FE cathodes. A low turn-on field of ∼3.4 V/μm was obtained from the NW arrays, which is impressively lower than that from other reported values. The results reported in this work give direction to the development of a facile growth technique for PZT NWs over large surfaces and also are of interest to the generation of high current electron beam from FE NW based cathodes for field emitter applications.

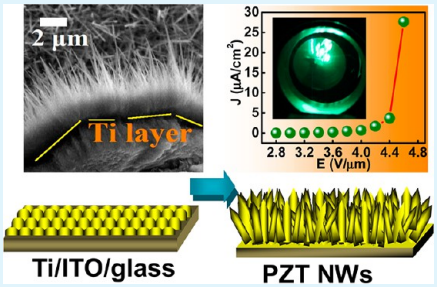

KEYWORDS: *PZT, nanowires, hydrothermal, field emission, ferroelectric*

INTRODUCTION

Ferroelectric (FE) perovskite oxides continue to be an important class of materials because of their high dielectric and piezoelectric coefficients and switchable nonvolatile polarization properties.[1−4] Among the state-of-the-art perovskite oxide materials, lead zirconium titanate with the specific composition of $Pb(Zr_{0.52}Ti_{0.48})O_3$ (PZT) exhibits the highest piezo and ferro-coefficients and is of great technological interest for applications as piezoelectric transducers, pyroelectric sensors, high-dielectric capacitors, and nonvolatile memory devices.[5−8] Most frequently, PZT is used in the form of single crystals, polycrystalline bulk ceramics, and thin films in microelectronics devices[4,9,10] and in miniaturized FE random access memory (FRAM) devices.[11−13]

One-dimensional (1D) nanostructures such as nanowires (NWs) with tunable size, morphology, phase, and crystallographic orientation have become the focus of intensive research owing to their unique diameter and orientation dependent electrical properties.[14,15] Due to the novel and improved properties, 1D nanostructures therefore have intrinsic priorities over conventional thin films and PZT is not far behind.[8,16−25] Recent research activities on PZT 1D nanostructures have indicated huge enhancement of piezoelectric properties useful for sustainable micro/nanopowering sources.[8,16−25] FE PZT nanotubes with controlled orientation were reported to be attractive candidates for next-generation nonvolatile random access memories.[19] In order to have exciting opportunities of fundamental research and innovative applications of PZT nanostructures, the development of a facile method is necessary for fabricating high quality, low dimensional nanostructures over large areas. However, to date large-scale fabrication methods of PZT nanostructures have been restricted in accessibility due to their complicated methodologies and high-cost. So far, PZT NWs[8] and nanotubes[19] have been selectively grown by hydrothermal processes and a combined template-directed sol−gel method with a spin-coating technique on Nb doped strontium titanium oxide ($SrTiO_3$:Nb)[8] and platinized silicon substrates,[19] respectively. These methods are indeed compelling, but alternative low cost, easily accessible methods that can be used to grow PZT 1D nanostructures over large surface areas are required to be explored that may expand the outreach of probes for understanding the structure−

Received: April 8, 2013
Accepted: June 11, 2013
Published: June 11, 2013

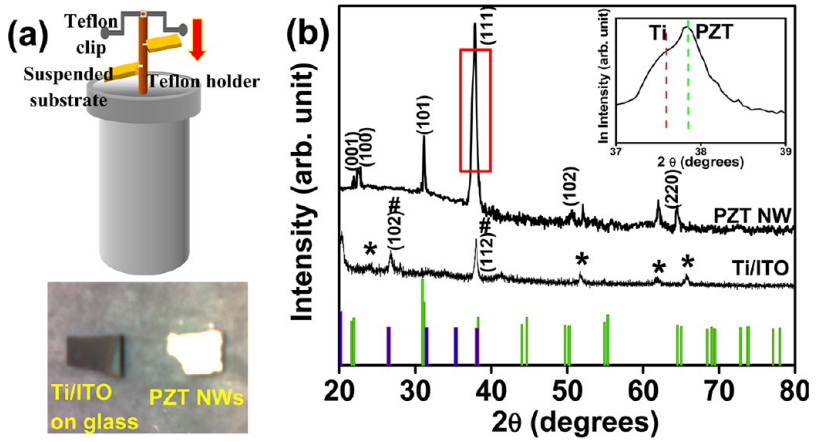

Figure 1. (a) Upper panel experimental setup with the suspended Ti/ITO/glass substrates inserted inside the Teflon chamber in a typical hydrothermal reaction process. Lower panel photographs of the Ti/ITO/glass substrate and the final PZT NWs product on the same. (b) XRD spectra of the Ti/ITO/glass and PZT NWs on the same. ITO substrate peaks (*) and the Ti peaks (#) are shown in the Ti/ITO/glass spectrum. The (111) peak in the PZT NW XRD spectrum is deconvoluted to show the Ti bottom layer peak and the PZT peak in log scale. Standard database of PZT (green bar) and Ti (red bar) are also shown for comparison.

property relations in PZT nanostructures for future advancement in memory technologies.

Demonstration of nanostructure based FE field emitters have been the center of attention because of their technological importance in fabrication of various devices such as flat panel displays, electron sources in vacuum microelectronics, and so forth.[26,27] Quantum tunnelling of injected electrons from the materials surface into vacuum under the influence of strong electrostatic field (10^6–10^7 V/cm) is called field emission. Nanostructured FE field emitters show capability to deliver high emission current density with excellent current stability and low turn-on voltage.[26] Numerous 1D nanostructures have been synthesized and studied as field emitters with a view to obtain a large current density at relatively lower applied voltages.[28−37] Traditional FE materials hold promise to be used as excellent electron sources due to the inversion of the spontaneous polarization in these materials.[38] Since electrons and holes are present on both sides of a FE material to compensate for the spontaneous polarization, it is predicted that a high density of compensated electrons could be emitted from the FE materials' surface under an external applied field.[38] It was understood that the FE field emitters may offer a source of high current density electron beams for applications where the use of conventional cathodes is limited by the required current density, cathode poisoning, or lifetime.[38] There is now considerable interest in the FE cathodes as electron sources for low power devices such as emissive flat panel displays. Field emission studies of FE materials have been investigated by various groups.[39,40] However, the voltages needed to produce electron emission from existing FE cathodes are still in the range of hundreds to thousand of volts. Early observations of electron emission were reported by Belayev and Bendrikova.[41] Subsequently, electron emission was investigated in various FE materials, including $LiNbO_3$ and $LiTaO_3$.[42,43] The emission current density observed from all of the above-mentioned materials was $<10^{-9}$ A/cm^2, which is practically too low for many device applications such as electron sources for electron accelerators and flat panel displays. To this end, PZT with its excellent piezoelectric and FE properties offers to act as a finite electron source. During the past few years, the volume of literature on electron emission from PZT surfaces has increased rapidly.[39,42−48] Recently field emission current has been reported from PZT nanoemitters which were prepared by coating nanometer thick PZT films on single-crystal silicon islands.[48] However, to our knowledge, field emission behavior of as-grown PZT nanostructures has not yet been investigated.

In the present work, we report on the optimized growth of PZT NWs by a Ti seed layer assisted hydrothermal method using an integrated sputtering technique and hydrothermal process on indium titanium oxide (ITO) coated glass substrates (ITO/glass). The presence of Ti seed layer triggers the formation of PZT nanoislands (or nucleation sites) and ensures the formation of PZT NWs over a large surface area with well-controlled dimensions. Unlike other reported PZT NWs on either Ti foils,[20] which makes it unsuitable for device applications or on expensive STO:Nb substrates,[8] our approach ensures uniform and dense growth of PZT NWs over inexpensive glass substrates making them highly desirable for industrial customization. Second, the prepared PZT NWs have been investigated for potential field emission properties to provide a basic understanding of the electron emission behavior of PZT NW FE electrode surface. Due the smaller tip apex radius, PZT NWs are found to be quite suitable for field emission application as were reported for other 1D nanostructures.[26,27,31−35]

EXPERIMENTAL SECTION

Ti Seed Layer Deposition. We chose ITO coated sodalime glass as the substrate for the deposition of Ti seed layer and the subsequent growth of PZT NW arrays from them. It was noticed that the presence of ITO coating helped in the deposition of uniformly thick Ti layer on the glass substrate, which was otherwise not obtained on uncoated glass substrates. A radio frequency (RF) sputtering technique was used to deposit a thin layer of Ti seed layer on the substrates (Figure 1a, lower panel). Before Ti sputtering, the ITO/glass substrates were cleaned by ultrasonic bath using acetone, methanol and water, and N_2 dried in vacuum. Ti seed layer was deposited using a CRC-100 sputtering system (Plasma Sciences Inc.) with an ambient Ar gas pressure of 5 mTorr. Two deposition cycles each for 10 min were run by varying current from 100 to 150 mA to finally deposit 500 nm thick Ti particulate films. Deposition parameters (voltage, time and current) were optimized in order to grow uniformly thick, crack-free continuous Ti metal film. After each deposition, Ti seed layer was characterized by X-ray diffraction (XRD), performed by Bruker AXS

D8 diffractometer equipped with Lynx Eye position-sensitive detector and atomic force microscopy (AFM by Digital Instruments).

PZT NW Growth. All chemicals were used as is with a minimum of 99.99% ACS grade. Growth of PZT nanowire arrays were conducted on Ti seed layers using a hydrothermal process similar to that described by Lin et al.[20] In a typical synthesis process, the reaction solution was prepared by mixing 2 mmol of Ti–*n*-butoxide ($Ti(OCH_2CH_2CH_2CH_3)_4$) dissolved in 25 mL ethanol, and a stoichiometric amount of hydrated zirconium chloride ($ZrOCl_2{\cdot}8H_2O$) dissolved in 25 mL deionized water, separately. Ti ion containing ethanol solution was then added slowly into the Zr ion containing aqueous solution under vigorous stirring. In the next step, 200 mL of NH_4OH solution containing 28–30% of NH_3 was added to this mixture that resulted in a precipitation of intermediate hydroxide phase ($Zr_{0.52}Ti_{0.48}O(OH)_2$). The precipitate was washed and centrifuged several times with water and ethanol in order to remove unreacted chemicals and ionic byproducts. After thorough cleaning, the hydroxide precipitate was redispersed in 36 mL of deionized water. To this solution stoichiometric quantity of hydrated lead nitrate $Pb(NO_3)_2{\cdot}8H_2O$, 0.02 g PVA (poly(vinyl alcohol)), and 0.4 g PAA (poly(acrylic acid)) were added successively. Required quantity of KOH pellets was added to this mixture to maintain an alkaline pH of ~12. This final growth solution was put into a Teflon lined hydrothermal vessel. Ti seed layer deposited ITO/glass substrates were suspended freely midway inside the Teflon chamber using a custom designed clip-on Teflon holder (Figure 1a, upper panel). The hydrothermal reactants were then sealed and placed in the preheated oven at 200 °C for 16 h. After completion of the reaction, the chamber was air cooled and the substrates were cleaned with deionized water and ethanol. The presence of uniform, thin white layers on the substrates were indicative of the growth of PZT NWs (Figure 1a, lower panel). Microstructural characterization of PZT NWs was carried out by scanning electron microscopy (SEM, JEOL JSM 6390 LV) and high resolution transmission electron microscopy (TEM-HRTEM, FEI Tecnai F20 S-Twin TEM). Composition analysis was done by energy-dispersive X-ray spectroscopy (EDS, Oxford Instruments INCAX sight) equipped with the SEM. For TEM measurements, the PZT NWs were carefully scrapped out and then dispersed in isopropyl alcohol. A few drops of this solution were then deposited on a carbon coated copper grid and air-dried.

Field Emission Measurement. The field emission current density–applied field (J–E) and current–time (I–t) measurements were carried in all metal field emission microscope. The field emission studies were carried out in a "close proximity" (also termed as "planar diode") configuration, wherein the PZT NW arrays grown on to the ITO/glass substrate served as the cathode and a semitransparent cathodoluminescent phosphor screen as the anode. Provision of back contact was done using highly conducting carbon tape from copper rod, and this whole assembly was held in front of the anode (screen) at a distance of ~1 mm. The working chamber was evacuated using an ultrahigh vacuum system comprising of a rotary-backed turbo molecular pump, a sputter ion pump, and a titanium sublimation pump. The cathode (PZT NWs) did not show any appreciable degassing and vacuum could be obtained with usual speed. After baking the system at 150 °C for 8 h, a base pressure of $\sim 1 \times 10^{-8}$ mbar was obtained. The J–E measurement was carried out at this base pressure using a Keithley 485 Picoammeter and a Spellman high voltage DC power supply. Special care was taken to avoid any leakage current by using shielded cables with proper grounding.

RESULTS AND DISCUSSION

Representative XRD spectra of the Ti coated ITO/glass (Ti/ITO/glass) substrates and that of the PZT NWs deposited on Ti coated ITO/glass are shown in Figure 1b. Standard XRD patterns for Ti (JCPDS card: 00-044-1294) and tetragonal PZT (JCPDS card: 01-070-4060) are shown for comparison. Both Ti coated ITO/glass and the PZT NWs samples show polycrystalline patterns without any preferential orientation. The XRD patterns indicate that the samples are phase pure with no peaks from secondary phase formation within the resolution limits of the XRD. Absence of most of the Ti and ITO peaks in the XRD pattern of the PZT NW sample is suggestive of the densely covered growth of the NWs on the substrate. Since the 2θ value of the (111) peak in tetragonal PZT closely matches with that of the (112) plane in hexagonal Ti, we deconvoluted the (111) XRD peak of PZT NW pattern. Two peaks, one for the Ti and the other for the PZT, were observed after deconvolution (shown in log scale in the inset to Figure 1b). The ratio of the normalized intensities of the Ti/PZT peaks is as low as ~0.005 which indicates good coverage of the NWs in the sample.

Surface morphology of the Ti coating after sputtering was studied by AFM (Figure 2a). The as-deposited Ti film exhibits a uniform and flat surface with a low root-mean-square value of surface roughness (R_{rms}) of 10 ± 2 nm. The average grain size

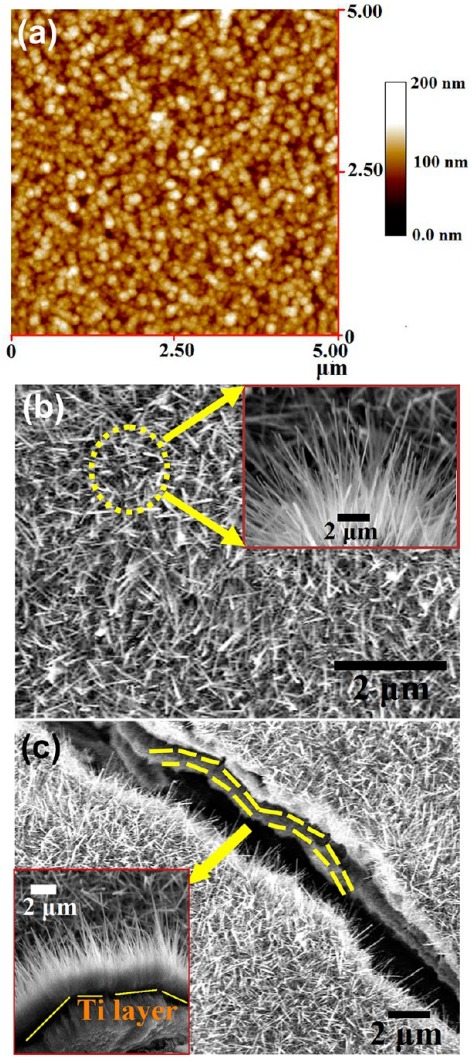

Figure 2. (a) AFM image showing the surface morphology of the Ti coating on the ITO/glass substrate used as the seed layer in the hydrothermal growth of PZT NWs. (b) SEM image of the PZT NW arrays showing uniform and continuous coverage over large surface area. (inset) SEM image of the titled substrate indicating that the NWs have grown upright to the substrate with random orientation. (c) SEM image showing a region of the PZT NW arrays that was forcefully cracked to expose the bottom Ti seed layer that promoted the upright growth of the PZT NWs. (inset) Upright growth of PZT NWs from Ti seed layer from the cracked zone.

dx.doi.org/10.1021/am4012879 | ACS Appl. Mater. Interfaces 2013, 5, 6261–6267

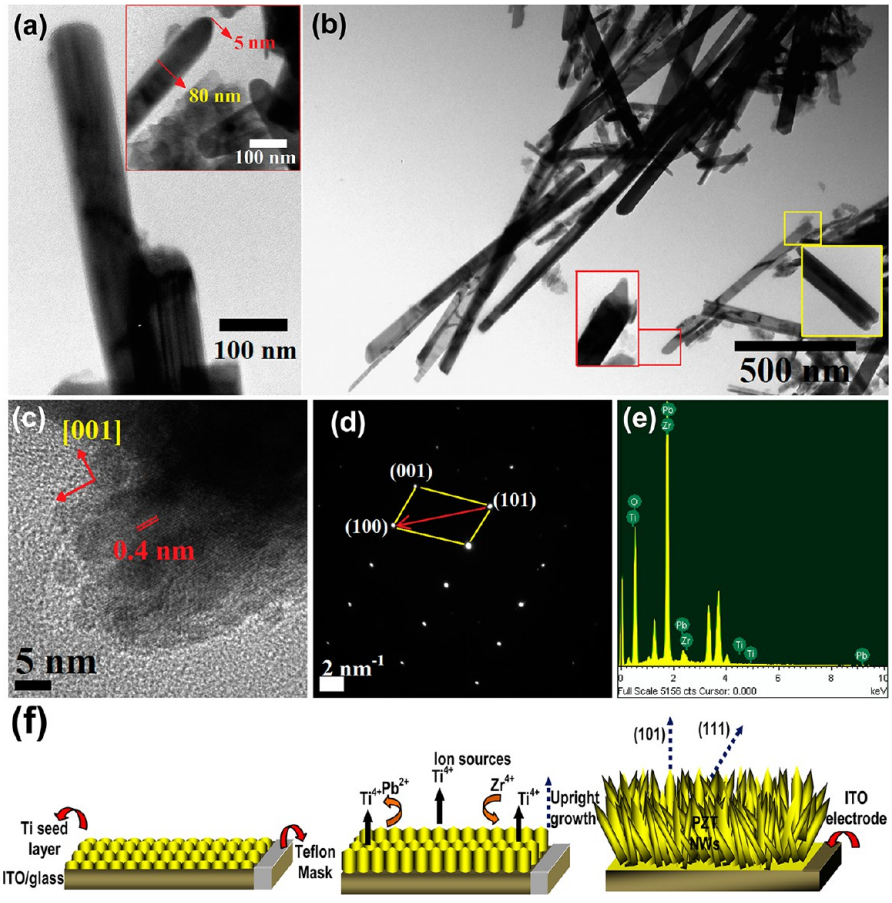

Figure 3. (a, b) TEM images of the PZT NWs. (insets) Morphology of the tip and the base of individual NWs. (c) HRTEM image of a single PZT NW near its tip. (d) SAED pattern collected from an individual PZT NW showing single crystal pattern with marked crystal planes in the tetragonal PZT lattice structure. (e) Representative EDS spectrum collected from different zones of a single PZT NW. (f) Schematic diagram showing the step-by-step growth of PZT NW arrays on Ti coated ITO/glass substrate.

measured is around 90 ± 12 nm with a film thickness of 500 ± 10 nm as measured by a profilometer. SEM image of the PZT NWs deposited on Ti/ITO/glass substrates is shown in Figure 2b. The image shows uniform and continuous growth of densely populated PZT NWs with a large aspect ratio (>60) and without any exposed Ti bottom layer or ITO/glass substrate. Inset to Figure 2b shows a titled image of an array of the PZT NWs, which suggests that the NWs have grown upright to the substrate with random orientation. A part of the PZT NW film was forcefully cracked, and the bottom Ti layer was exposed and observed under SEM (Figure 2c). It was evident that the PZT NWs grew upright from the bottom Ti layer which acted as the seed layer promoting the growth of the NWs (inset to Figure 2c).

Figure 3 shows the TEM images of the PZT NWs. The NWs have sharp boundaries and uniform lengths with an average diameter of 80 ± 5 nm. As shown in the inset to Figure 3a, and insets to Figure 3b, the majority of the NWs have rounded or tapered tip with an average tip diameter of 5 ± 2 nm. On the basis of the observation of around 50 different NWs, it appears that the bases of the NWs are tetragonal in shape which demonstrates the inherent crystal structure of PZT. The HRTEM image of a single NW near its tip is shown in Figure 3c. As indicated, the continuous and sharp lattice fringe spacing in the NW match with the (001) plane of tetragonal PZT. The particulate features at the tip are due to the surface disintegration of the NW upon long exposure to the high energy electron beam during the TEM imaging. The selected area electron diffraction (SAED) pattern collected from an individual PZT NW shows a single crystal pattern with marked crystal planes in the tetragonal lattice structure (Figure 3d). The SAED pattern also indicates that the NWs are of high crystalline nature without the presence of detectable structural defects. EDS spectra collected from different zones of a single PZT NW (Figure 3e) reveal stoichiometric composition within an error limit of 0.001 at %.

The design to grow PZT NWs from Ti seeds hence proves to be effective. As observed, the diameter of the NWs is commensurate with the grain size calculation from the AFM, which surely suggests that the Ti seeds act as individual nucleation sites for the initiation of the growth of the PZT NW on the ITO/glass substrate. The step by step growth process has been schematically illustrated in Figure 3f. The study indicated that the substrate position was crucial to the growth of PZT NWs with uniform sizes on the substrate. When the Ti/ITO/glass substrate was kept at the bottom of the Teflon container, large PZT microrods (1−2.5 μm in diameter) were obtained instead (Figure 4a). It can be assumed that PZT microrods may have grown by Oswald ripening from NWs at higher precursor concentration near the bottom of the Teflon chamber after an elapsed period of reaction time.[14,15] We have earlier observed that it is possible to grow sulfide NWs upright to the substrate using metal foils as the source and substrate in the solvothermal process where the metallic source at the

dx.doi.org/10.1021/am4012879 | ACS Appl. Mater. Interfaces 2013, 5, 6261−6267

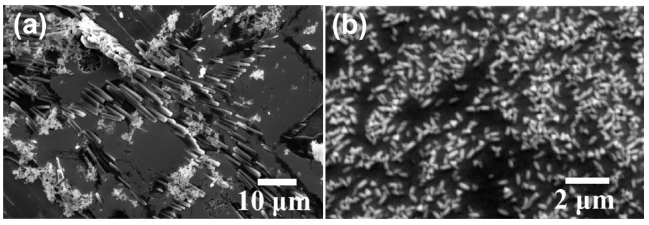

Figure 4. (a) SEM image showing PZT microrods (1−2.5 μm in diameter) formed on Ti coated ITO/glass substrates positioned at the bottom of the Teflon container during the hydrothermal process. (b) SEM image showing the PZT nanorods (average diameter 150 nm) with average aspect ratio of <5 in case where no Ti seed layer was deposited on the ITO/glass substrate.

bottom helps in the vertical growth of the NWs by facilitating unidirectional supply of the precursor ions from the base to the top of the NWs.[32,49] Unidirectional upright growth of other materials are also feasible via electrochemical deposition and gas−solid process on metal coated glass substrates.[50] Following a similar growth mechanism, in this case, upward flow of Ti ions from the Ti seeds on the substrate and the supersaturation of Ti precursor ions in the growth solution attribute to the upright anisotropic growth of PZT NWs through homogeneous nucleation (scheme shown in Figure 3f). In order to verify our idea, we carried out a contrastive experiment to grow PZT NWs without coating of Ti metal on ITO/glass substrate. As expected, there was no upright growth of PZT NWs on the ITO substrate. Insignificant 1D growth of small PZT nanorods was noticed in this case (average diameter 150 nm) with average aspect ratio of <5 (Figure 4b).

In order to understand the electron emissive properties we carried out field emission measurements of the PZT NWs/Ti/ITO/glass sample. The J−E characteristics of the PZT NWs are depicted in Figure 5a. The turn-on field, defined as the field required to draw an emission current of 0.1 μA/cm^2, is found to be 3.4 V/μm, which is 2-fold lower that the turn-on field observed in PZT coated Si nanoemitter.[48] As the applied voltage is increased further, the emission current is increased very rapidly and an emission current density of ∼27 μA/cm^2 has been drawn at an applied field of ∼4.6 V/μm. The applied field E is defined as $E = V/d$, where V is the applied voltage and d is the separation between the anode and the emitter cathode (PZT NWs sample). In general, this field is also referred to as an average field. In the present case, the current density J is estimated by considering the entire area of the emitter 0.5 cm^2 (i.e., the area of the Ti coated substrate as the NWs grew uniformly all over the substrate). The Fowler−Nordheim (F−N) plot, i. e. $\ln(J/E^2)$ versus $(1/E)$, derived from the observed J−E characteristic is shown in Figure 5b. The F−N plot shows deviation from linearity. The observed nature of F−N plot is observed to be quite similar to the published data for well-explored inorganic semiconductors.[29,31]

Various field emission theories/models have been proposed for bulk PZT materials.[39,44−48] The general view is that a FE material when appropriately polarized will have the positive charges of the dipoles oriented toward the FE surface. The resulting net positive charge on the surface is compensated by electrons, whose origin is still a matter of debate in order to preserve charge neutrality.[32] Upon fast reversal of the polarization, the negative charges of the FE dipoles orient toward the surface of the FE material, leading to a rapid build-up of a repulsive electrostatic force which is responsible for the ejection of electrons from the surface. The brief emission mechanism presented above constitutes a simplified view of a complex phenomenon. It is relevant to point out that the

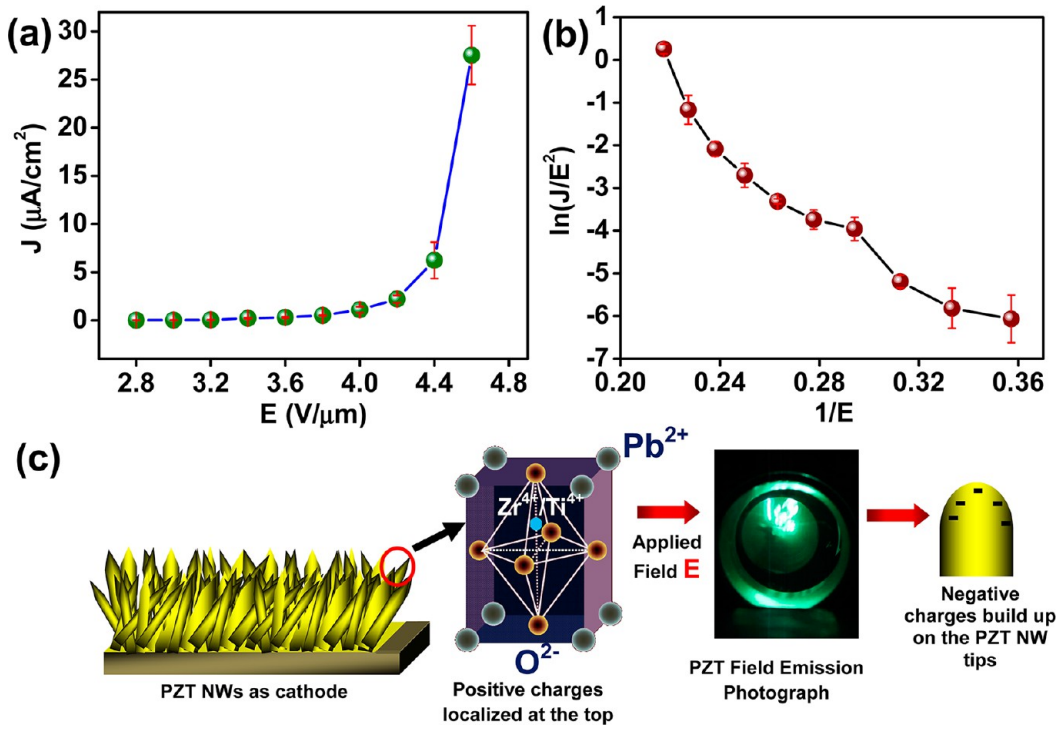

Figure 5. (a) Current density−applied field (J−E) characteristics of the PZT NWs. (b) Plot of the Fowler−Nordheim (F−N) relation, i. e. $\ln(J/E^2)$ versus $(1/E)$, as derived from the observed J−E characteristics in part a. (c) Schematic diagram illustrating the mechanism of field emission of PZT NW arrays. The green emission is seen in an actual photograph captured during the measurement.

dx.doi.org/10.1021/am4012879 | ACS Appl. Mater. Interfaces 2013, 5, 6261−6267

electron emission mechanism may be quite different from the one mentioned above,[51] and also for PZT bulk materials researchers have reported the nonuniversal phenomenon of the field electron emission. However, the vast literature survey indicates that there is no data in regards to the field emission study of the PZT NWs and hence, for the scientific and technological advancement, exploration of the aforesaid material as a field emitter is essential and also further study is needed in this direction. As an initiation of such research direction, our report on the field emission behavior in PZT NWs grown on inexpensive glass substrates holds great promise for future technological advancement in FE materials research. The next step of this research could be directed to study the roles of dimensions (both length and diameter) and alignment of the PZT NWs on the field emission properties of PZT NW cathodes by varying the grain size of the Ti bottom layer and studying their effects on the parameters of the hydrothermal reaction. Moreover studying the field emission properties of the PZT NWs under pulsating electric field may provide fundamental understanding to the research of FE NW based field emitters.

CONCLUSIONS

In conclusion, FE PZT NW upright arrays were grown over a large surface area on ITO/glass substrate directed by Ti seed layer at the bottom. The Ti seed layer was first deposited through a controlled RF sputtering process which was then used as a substrate for the growth of large scale PZT NW arrays through an optimized hydrothermal process. Position of the Ti/ITO/glass substrate and the presence of Ti coating were found to affect the uniform growth and coverage of the single crystalline NWs. We also investigated the field emission properties of the as grown PZT NWs using FE NW films as the cathodes. Compared to the scarcely reported data of PZT nanoemitters, our carefully designed PZT NWs showed a quite low turn-on field of ~3.4 V/μm with a relatively large current density of ~27 μA/cm^2. The results reported in this work offers a platform for introducing newer techniques for the growth of 1D PZT nanostructures and expand the investigation of the fundamental structural and field emission properties of this FE NW based cathodes.

AUTHOR INFORMATION

Corresponding Author

*E-mail: datta@usf.edu.

Notes

The authors declare no competing financial interest.

ACKNOWLEDGMENTS

This work was partially supported by the Florida Cluster for Advanced Smart Sensor Technologies and the United States Army (Grant No. W81XWH1020101/3349). D.S.J and R.V.K. would like to thank CSIR, New Delhi, India, for Emeritus Scientist and SRF schemes, respectively. The field emission work has been carried out as a part of CNQS-UPE-UGC program activity.

REFERENCES

(1) Imada, M.; Fujimori, A.; Tokura, Y. *Rev. Mod. Phys.* **1998**, *70*, 1039−1263.
(2) Goodenough, J. B. *Prog. Solid State Chem.* **1971**, *5*, 145−399.
(3) Setter, N.; Damjanovic, D.; Eng, L.; Fox, G.; Gevorgian, S.; Hong, S.; Kingon, A.; Kohlstedt, H.; Park, N. Y.; Stephenson, G. B.; Stolitchnov, I.; Taganstev, A. K.; Taylor, D. V.; Yamada, T.; Streiffer, S. *J. Appl. Phys.* **2006**, *100*, 051606−051652.
(4) Martin, L. W.; Chu, Y.-H.; Ramesh, R. *Mater. Sci. Eng.: R* **2010**, *68*, 89−133.
(5) Scott, J. F.; Paz de Araujo, C. A. *Science* **1989**, *246*, 1400−1405.
(6) Schwarzkopf, J.; Foranari, R. *Prog. Cryst. Growth Charact. Mater.* **2006**, *52*, 159−212.
(7) Guo, R.; Cross, L. E.; Park, S. E.; Noheda, B.; Cox, D. E.; Shirane, G. *Phys. Rev. Lett.* **2000**, *84*, 5423−5426.
(8) Xu, S.; Hansen, B. J.; Wang, Z. L. *Nat. Commun.* **2010**, *1*, 93−97.
(9) Liu, W.; Jiang, B.; Zhu, W. *Appl. Phys. Lett.* **2000**, *77*, 1047−1049.
(10) Izyumskaya, N.; Alivov, Y. I.; Cho, S. J.; Morkoç, H.; Lee, H.; Kang, Y. S. *Crit. Rev. Solid State Mater. Sci.* **2007**, *32:3*, 111−202.
(11) Mukherjee, D.; Hordagoda, M.; Bingham, N.; Srikanth, H.; Mukherjee, P.; Witanachchi, S. *J. Appl. Phys.* **2012**, *112*, 064101−064108.
(12) Mukherjee, D.; Hyde, R.; Mukherjee, P.; Srikanth, H.; Witanachchi, S. *J. Appl. Phys.* **2012**, *111*, 064102−064112.
(13) Mukherjee, D.; Hyde, R.; Dhakal, T.; Srikanth, H.; Mukherjee, P.; Witanachchi, S. *Mater. Res. Soc. Symp. Proc.* **2009**, *1199*, 37−43.
(14) Xia, Y.; Yang, P.; Sun, Y.; Wu, Y.; Mayers, B.; Gates, B.; Yin, Y.; Kim, F.; Yan, H. *Adv. Mater.* **2003**, *15*, 353−389.
(15) Zhai, T.; Yao, J. In *One-Dimensional Nanostructures: Principles and Applications*; John Wiley & Sons: New York, 2012; ISBN 978-1-118-07191-5.
(16) Zhang, X. Y.; Zhao, X.; Lai, C. W.; Wang, J.; Tang, X. G.; Dai, J. Y. *Appl. Phys. Lett.* **2004**, *85*, 4190−4192.
(17) Xu, G.; Ren, Z. H.; Du, P. Y.; Weng, W. J.; Shen, G.; Han, G. R. *Adv. Mater.* **2005**, *17*, 907−910.
(18) Wang, J.; Sandu, C. S.; Colla, E.; Wang, Y.; Ma, W.; Gysel, R.; Trodahl, H. J.; Setter, N.; Kuball, M. *Appl. Phys. Lett.* **2007**, *90*, 133107−133109.
(19) Kim, J.; Yang, S. A.; Choi, Y. C.; Han, J. K.; Jeong, K. O.; Yun, Y. J.; Kim, D. J.; Yang, S. M.; Yoon, D.; Cheong, H.; Chang, K. S.; Noh, T. W.; Bu, S. D. *Nano Lett.* **2008**, *8*, 1813−1818.
(20) Lin, Y. R.; Liu, Y. T.; Sodano, H. A. *Appl. Phys. Lett.* **2009**, *95*, 122901−122903.
(21) Chen, X.; Xu, S.; Yao, N.; Shi, Y. *Nano Lett.* **2010**, *10*, 2133−2137.
(22) Nguyen, T. D.; Nagarah, J. M.; Qi, Y.; Nonnenmann, S. S.; Morozov, A. V.; Li, S.; Arnold, C. B.; McAlpine, M. C. *Nano Lett.* **2010**, *10*, 4595−4599.
(23) Qi, Y.; Kim, J.; Nguyen, T. D.; Lisko, B.; Purohit, P. K.; McAlpine, M. C. *Nano Lett.* **2011**, *11*, 1331−1336.
(24) Xiao, Z.; Ren, Z.; Liu, Z.; Wei, X.; Xu, G.; Liu, Y.; Li, X.; Shen, G.; Han, G. *J. Mater. Chem.* **2011**, *21*, 3562−3564.
(25) Tang, H.; Lin, Y.; Andrews, C.; Sodano, H. A. *Nanotechnol.* **2011**, *22*, 015702−015709.
(26) Zhai, T.; Li, L.; Ma, Y.; Liao, M.; Wang, X.; Fang, X.; Yao, J.; Bando, Y.; Golberg, D. *Chem. Soc. Rev.* **2011**, *40*, 2986−3004.
(27) Joag, D. S.; More, M. A.; Sheini, F. J. In *Nanowires - Implementations and Applications*; InTech: New York, 2011; Chapter 24, ISBN 978-953-307-318-7.
(28) Kakade, B. A.; Pillai, V. K.; Late, D. J.; Chavan, P. G.; Sheini, F. J.; More, M. A.; Joag, D. S. *Appl. Phys. Lett.* **2010**, *97*, 073102−073104.
(29) Zhu, Y. W.; Zhang, H. Z.; Sun, X. C.; Feng, S. Q.; Xu, J.; Zhao, Q.; Xiang, B.; Wang, R. M.; Yu, D. P. *Appl. Phys. Lett.* **2003**, *83*, 144−146.
(30) Wang, W.; Zeng, B.; Yang, J.; Poudel, B.; Huang, J.; Naughton, M. J.; Ren, Z. *Adv. Mater.* **2006**, *18*, 3275−3278.
(31) Chavan, P. G.; Badadhe, S. S.; Mulla, I. S.; More, M. A.; Joag, D. S. *Nanoscale* **2011**, *3*, 1078−1083.
(32) Datta, A.; Chavan, P. G.; Sheini, F. J.; More, M. A.; Joag, D. S.; Patra, A. *Cryst. Growth Design* **2009**, *9*, 4157−4162.
(33) Panda, S. K.; Datta, A.; Sinha, G.; Chaudhuri, S.; Chavan, P. G.; Patil, S. S.; More, M. A.; Joag, D. S. *J. Phys. Chem. C* **2008**, *112*, 6240−6244.
(34) Sinha, G.; Datta, A.; Panda, S. K.; Chavan, P. G.; More, M. A.; Joag, D. S.; Patra, A. *J. Phys. D: Appl. Phys.* **2009**, *42*, 185409−185415.

(35) Sinha, G.; Panda, S. K.; Datta, A.; Chavan, P. G.; Shinde, D. R.; More, M. A.; Joag, D. S.; Patra, A. *ACS Appl. Mater. Inter.* **2011**, *3*, 2130−2135.
(36) He, J. H.; Wu, T. H.; Hsin, C. L.; Li, K. M.; Chen, L. J.; Chueh, Y. L.; Chou, L. J.; Wang, Z. L. *Small* **2006**, *2*, 116−120.
(37) Zhou, J.; Deng, S. Z.; Nu, N. S.; Chen, J.; She, J. C. *Appl. Phys. Lett.* **2003**, *83*, 2653−2655.
(38) Rosenman, G.; Rez, I. *J. Appl. Phys.* **1993**, *73*, 1904−1908.
(39) Zhang, W.; Huebner, W.; Sampayan, S. E.; Krogh, M. L. *J. Appl. Phys.* **1998**, *83*, 6055−6060.
(40) Kim, Y. T.; Yoon, K. H.; Kim, T. H.; Park, K. B. *Appl. Phys. Lett.* **1999**, *75*, 1964−1966.
(41) Belayev, L. M.; Bendrikova, G. C. *Fiz. Tverd. Tela (Leningrad)* **1964**, *6*, 645; *Sov. Phys. Solid State* **1964**, *6*, 506.
(42) Rosenblum, B.; Braunlich, P.; Carrico, J. P. *Appl. Phys. Lett.* **1974**, *25*, 17−19.
(43) Rosenman, G. I.; Boikova, E. I. *Phys. Stat. Solidi A* **1980**, *58*, 379−384.
(44) Takamuro, D.; Takao, H.; Sawada, K.; Ishida, M. *Sens. Act. A* **2004**, *114*, 230−235.
(45) Angadi, M.; Auciello, O.; Krauss, A. R.; Gundel, H. W. *Appl. Phys. Lett.* **2000**, *77*, 2659−2661.
(46) Flechtner, D.; Golkowski, C.; Ivers, J. D.; Kerslick, G. S.; Nation, J. A.; Schächter, L. *J. Appl. Phys.* **1998**, *83*, 955−961.
(47) Auciello, O.; Ray, M. A.; Palmer, D.; Duarte, J.; McGuire, G. E.; Temple, D. *Appl. Phys. Lett.* **1995**, *66*, 2183−2185.
(48) Fletcher, P. C.; Mangalam, V. K. R.; Martin, L. W.; King, W. P. *J. Vac. Sci. Technol. B* **2013**, *31*, 021805−021810.
(49) Datta, A.; Gorai, S.; Panda, S. K.; Chaudhuri, S. *Cryst. Growth Design* **2006**, *6*, 1010−1013.
(50) Datta, A.; Panda, S. K.; Gorai, S.; Ganguli, D.; Chaudhuri, S. *Mater. Res. Bull.* **2008**, *43*, 983−989.
(51) Gundel, H. In *Science and Technology of Electroceramic Thin Films*; Kluwer Academic Publishers: Netherlands, 1995; pp 335−351.